Strength of the scissors mode in odd-mass Gd isotopes from the radiative capture of resonance neutrons

J. Kroll,[1,*] B. Baramsai,[2] G. E. Mitchell,[2] U. Agvaanluvsan,[3] F. Bečvář,[1] T. A. Bredeweg,[4] A. Chyzh,[2] A. Couture,[4] D. Dashdorj,[3] R. C. Haight,[4] M. Jandel,[4] A. L. Keksis,[4] M. Krtička,[1] J. M. O'Donnell,[4] W. Parker,[5] R. S. Rundberg,[4] J. L. Ullmann,[4] S. Valenta,[1] D. J. Vieira,[4] C. Walker,[2] and C. Y. Wu[5]

[1]*Charles University in Prague, CZ-180 00 Prague 8, Czech Republic*

[2]*North Carolina State University, Raleigh, North Carolina 27695, USA and Triangle Universities Nuclear Laboratory, Durham, North Carolina 27708, USA*

[3]*MonAme Scientific Research Center, P.O.Box 24-603, Ulaanbaatar, Mongolia*

[4]*Los Alamos National Laboratory, P.O. Box 1663, Los Alamos, New Mexico 87545, USA*

[5]*Lawrence Livermore National Laboratory, Livermore, California 94551, USA*

(Received 27 June 2013; published 19 September 2013)

Radiative neutron capture reaction was measured in the resolved resonance region for ^{152,154,156,158}Gd targets with the Detector for Advanced Neutron Capture Experiments γ-ray calorimeter at the Los Alamos Neutron Science Center. The γ-ray energy spectra for different multiplicities were obtained for several s-wave resonances in each nucleus. These spectra were analyzed within the extreme statistical model to provide unique information on the photon strength functions and especially on the scissors mode in odd Gd isotopes. The main result of this analysis is that in all nuclei scissors-mode resonances are built on excited levels and not only on their ground states. The strength of the mode found in ^{153}Gd and ^{155}Gd is comparable to the strength observed in well-deformed even-even Gd isotopes while it is substantially higher in ^{157,159}Gd. The difference in observed strengths of the scissors mode indicates an existence of an even-odd effect in this quantity.

DOI: 10.1103/PhysRevC.88.034317 PACS number(s): 25.40.Lw, 28.20.Np, 21.10.Ma, 23.20.Lv

I. INTRODUCTION

In medium and heavy mass nuclei detailed information about the properties of nuclear levels and transitions between them usually exists only at low excitation energies. In this region the spacing between levels is sufficient to observe individual γ transitions and to place them in the level scheme. As the nuclear level density (NLD) rapidly increases with the excitation energy it becomes impossible to resolve transitions between individual levels and determine their intensities using the present state-of-the-art of γ spectroscopy.

It is believed that average γ-decay properties of levels in this region of high NLD can be described by the extreme statistical model in terms of the NLD and a set of photon strength functions (PSFs) for different types and multipolarities of transitions. Knowledge on these quantities is important for the correct description of reaction rates in many different reactions and is especially needed in nuclear astrophysics and in the development of advanced nuclear reactors.

One of the ways to examine PSFs and NLD at excitation energies up to the neutron separation energy is via study of the properties of spectra of γ rays accompanying neutron capture at isolated neutron resonances. The subject of this paper is analysis of these spectra measured for ^{152,154,156,158}Gd targets at isolated s-wave neutron resonances using the highly segmented Detector for Advanced Neutron Capture Experiments (DANCE) detector array [1,2] installed at the pulsed neutron beam at the Los Alamos Neutron Science Center (LANSCE) at Los Alamos National Laboratory [3]. Neutron resonances are resolved using the neutron time-of-flight (TOF) technique. Thanks to the high granularity of the DANCE array, we could measure the γ-ray spectra of interest separately for individual multiplicities of the observed γ cascades.

The primary aim of these measurements was to obtain information on the role of the scissors-mode (SM) magnetic-dipole nuclear vibration in the γ decay of *excited* heavy deformed nuclei and to clarify whether the strength of this type of vibration in odd nuclei is the same as in even-even nuclei. Our previous results for ^{155,157}Gd targets, based on the same method, which are addressing a wider range of problems concerning PSFs, have been published [4,5].

The existence of the SM, predicted from theory [6,7], has been confirmed in high-resolution electron inelastic scattering experiment at low momentum transfer on ^{156}Gd [8]. Much information on SM properties in even-even nuclei was obtained by analyzing the intensities of ground-state $M1$ transitions in (γ,γ') reaction [9]. These experiments established that the γ-ray energy at which the enhancement of $M1$ transitions due to the SM reaches a maximum in rare-earth nuclei is close to 3 MeV. In addition, it was found that the total reduced $M1$ strength, $\sum B(M1)\uparrow$, belonging to the SM is proportional to the square of the nuclear deformation [10] and reaches a maximum of $\approx 3\mu_N^2$. The SM strength observed in (γ,γ') experiments with odd nuclei represents only a fraction of the true strength due to difficulties in the analysis caused by the significantly higher NLD in these nuclei. As a consequence, properties of the SM in odd nuclei are not that well established.

In addition to (γ,γ') and (e,e') experiments, the SM was also studied via radiative neutron capture, and in $(^3\mathrm{He},^3\mathrm{He}'\gamma)$

*kroll@ipnp.troja.mff.cuni.cz

and (^{3}He,$\alpha\gamma$) reactions. Analysis of γ-ray spectra from radiative neutron capture [4,11,12] and from ^{3}He-induced reaction [13–15] demonstrated that the SM enhances not only the ground-state transitions, but also plays an important role in transitions between excited levels.

Moreover, the data from two-step cascades (TSCs) following thermal neutron capture in ^{162}Dy also indicated that the strength of the mode in odd ^{163}Dy is significantly higher than that in neighboring even-even nuclei [9], $\sum B(M1)\uparrow \approx 6\mu_N^2$ [11]. However, ^{3}He-induced reaction data do not seem to show any odd-even effect on the strength of the mode. The strength from these reactions in both even-even and odd nuclei is comparable to that obtained in Ref. [11]. The main goal of this paper is to shed more light on the behavior of the SM in odd Gd nuclei and to clarify whether the SM strength is stronger compared to that in even-even deformed nuclei.

In Sec. II the experimental technique used to measure the γ spectra with the DANCE calorimeter is described. The modeling of the statistical γ cascades, an important ingredient of our analysis, is described in Sec. III. The results of this analysis based on comparison of the measured and simulated γ-ray spectra are presented in Sec. IV and compared with other available experimental data in Sec. V. A summary is provided in Sec. VI.

II. EXPERIMENT

A detailed description of the experimental setup and the data processing steps has been published [4,16,17]; here we describe only the basic features related to obtaining the experimental spectra analyzed in this paper.

A. Setup

The experiment was performed at the neutron source LANSCE [18]. The pulsed 800 MeV H^- beam from the LANSCE linac was injected into the proton storage ring after being stripped to H^+ by a thin foil. The nominal proton current was 100 μA. The proton-pulsed beam is then extracted with a repetition rate of 20 Hz and strikes a tungsten spallation target. A white spectrum of neutrons with energies from subthermal up to about 1 MeV is obtained. These neutrons are sent to flight path 14 at the Manuel Lujan Jr. Neutron Scattering Center. The DANCE detector array is installed at 20 m on this flight path.

The DANCE spectrometer [1,2] is designed for studying neutron capture cross sections on small samples. DANCE consists of 160 BaF_2 scintillation crystals surrounding a sample and covering a solid angle of $\simeq 3.5\pi$. Each crystal serves as a γ spectrometer. A 6-cm thick ^{6}LiH shell is placed between the sample and the BaF_2 crystals in order to reduce the scattered neutron flux striking the crystals. The remaining background due to scattered neutrons that penetrate the ^{6}LiH shell and interact with the BaF_2 crystals is subtracted in the offline analysis. In addition to the BaF_2 crystals, the DANCE setup includes two detectors that are used to monitor the neutron flux—a proportional counter filled with BF_3 + Ar gas, and an n-type surface barrier Si detector, which views a thin layer of ^{6}LiF.

The DANCE acquisition system [19] is based on digitization of signals from all 160 detectors using four-channel Acqiris DC265 digitizers with a sampling rate of 500 megasamples per second.

Intensities of the fast ($\tau \approx 600$ ps) and the slow ($\tau \approx 600$ ns) components of the scintillation signal from a specific BaF_2 crystal are collected independently. The ratio of these two components of the signal is used for discrimination against the α background from natural radioactivity of Ra, which is inevitably present in the BaF_2 crystals [2].

For each detected neutron capture event the acquisition system recorded the neutron time-of-flight belonging to the event and the list of the crystals that fired simultaneously together with the corresponding detector pulse-height information. All of this information was stored in list mode for offline analysis.

The energy calibration of the individual DANCE crystals was performed with a combination of radioactive γ-ray sources: ^{137}Cs, ^{88}Y, and ^{22}Na and the intrinsic radioactivity in the BaF_2 crystals due to ^{226}Ra and its daughters. The latter calibration was conducted on a run-by-run basis to provide energy alignment of all crystals in the offline analysis.

The detection efficiency of the DANCE detector array for a 1 MeV γ ray is 86% and the total efficiency for detection of a photon from a cascade exceeds 95%. The energy resolution is about 16% and 7% for 1 and 6 MeV γ rays, respectively.

The ^{156}Gd and ^{158}Gd targets were prepared at the Oak Ridge National Laboratory as self-supporting metal foil. The ^{152}Gd and ^{154}Gd targets were prepared at Lawrence Livermore National Laboratory by electroplating enriched Gd on Be foil, which was glued to an aluminum ring. Isotopic composition and thickness of the targets are listed in Table I. Data were accumulated for about 100 hours for each target.

TABLE I. Information related to Gd targets. In addition to isotopic composition and the average thickness of the Gd targets used in the measurements, the neutron separation energy S_n of the product nucleus is given together with the range of sum energies used in the data processing ($E_\Sigma^{(\mathrm{used})}$), and the critical energy E_{crit} used in simulations.

Target	Isotope abundance (%)							Aver. thick.	S_n	$E_\Sigma^{(\mathrm{used})}$	E_{crit}
	^{152}Gd	^{154}Gd	^{155}Gd	^{156}Gd	^{157}Gd	^{158}Gd	^{160}Gd	(mg/cm^2)	(MeV)	(MeV)	(MeV)
^{152}Gd	42.49	4.38	15.93	13.91	7.82	9.56	5.91	1.0	6.247	5.4–6.4	0.58
^{154}Gd	0.05	67.34	21.11	5.65	2.24	2.32	1.29	1.0	6.435	5.8–6.6	0.66
^{156}Gd	0.01	0.11	1.96	93.79	2.53	1.20	0.41	10.3	6.360	5.4–6.5	0.81
^{158}Gd	0.1	0.1	0.96	1.7	3.56	92.0	1.82	9.3	5.943	5.2–6.2	0.71

B. Data reduction and analysis

To ensure that the signals from individual BaF_2 detectors belong to the same event, a condition that they occur in a 10 ns coincidence window was imposed.

Often an emitted capture γ ray does not deposit its full energy just in one crystal. Therefore the number of crystals that fire is usually higher than the true multiplicity of a γ cascade following the capture. In our approach all contiguous crystals that have fired during an event are combined into a cluster and considered as a response of the detector array to a single γ ray. Hereafter, the number of clusters observed in a capture event is referred to as the *cluster multiplicity* M. This multiplicity is much closer to the true multiplicity of the γ cascade of the event than is the *crystal multiplicity*, i.e., to the total number of crystals that fire.

In the offline analysis of the list-mode data, we determined the cluster multiplicity m and the γ-ray energies deposited in all clusters for each capture event. Using the information on the sum of deposited energies we then constructed the *sum-energy spectra* for different multiplicities m corresponding to strong s-wave neutron resonances, identified using the TOF technique. An example of sum-energy spectra is given in Fig. 1. the spin and parity assignment of these resonances is $J^\pi = 1/2^+$. The TOF spectrum after its transformation to a neutron-energy scale is shown in Fig. 2 for the ^{156}Gd target.

Each sum-energy spectrum consists of (i) a *full-energy peak*, occurring at the energy sum near the neutron separation energy, S_n, of a given (n,γ) reaction, and (ii) a low-energy tail that corresponds to γ cascades for which a part of the emitted energy escaped the detector array. In practice the position of the peak is slightly shifted down with respect to S_n due to a contribution of internal electron conversion for transitions between the lowest levels of the product Gd nuclei. The shape of the sum spectrum at low energies (<3 MeV) is strongly influenced by the background from natural β activity in the BaF_2 crystals for multiplicity $m = 2$. As only events with a sum of deposited energies exceeding 5 MeV are used in our analysis, see the intervals $E_\Sigma^{(\mathrm{used})}$ in Table I, the role of this background is not important.

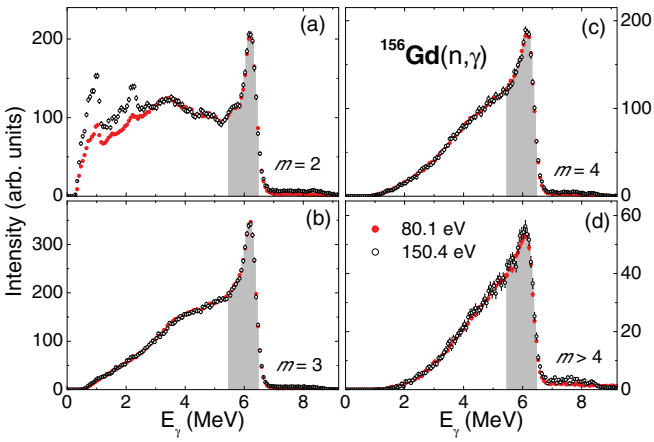

FIG. 1. (Color online) Experimental sum-energy spectra for cluster multiplicities $M \geqslant 2$ for two neutron resonances of ^{156}Gd target nucleus. Individual spectra were normalized as described in the text. Only events in the gray area were used for construction of MSC spectra.

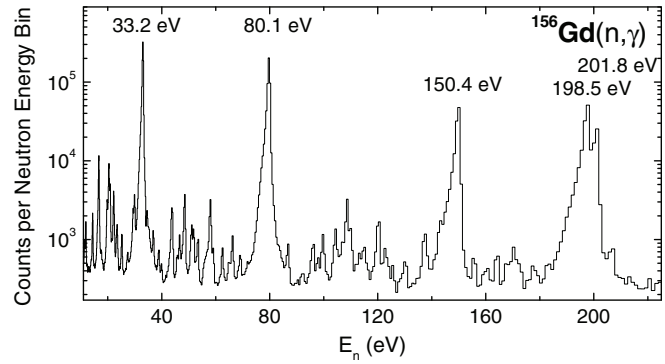

FIG. 2. Time-of-flight spectrum for ^{156}Gd target after its transformation to neutron-energy scale. There are 400 (exponentially distributed) neutron energy bins per decade. Only events corresponding to $m = 2$–7 and detected energy sum in the region of 5.4–6.5 MeV were considered.

As seen from Fig. 1, at energies exceeding S_n the intensities of sum-energy spectra are not zero. The dominant part of this effect, especially for low multiplicities, comes from the capture of scattered neutrons in Ba in the BaF_2 crystals. For higher multiplicities, there is also a small contribution from neutron captures on impurities in samples, which are mainly the odd isotopes ^{155,157}Gd.

We restricted our further analysis to events, which contribute to the full-energy peak in the sum-energy spectra. The ranges of sums of deposited energies, $E_\Sigma^{(\mathrm{used})}$, we chose for this purpose for individual (n,γ) reactions studied are specified in Table I. The range adopted for ^{157}Gd product nucleus is demarked in Fig. 1 by gray areas.

With these constraints we accumulated what we call *experimental multistep cascade* (MSC) *spectra*. For a given resonance, a MSC spectrum for multiplicity m was constructed by incrementing counts in the m bins corresponding to energies deposited in the m individual clusters for each event. The MSC spectra with sufficient statistics were obtained for (i) seven resonances of ^{152}Gd at 12.4, 36.9, 39.3, 42.7, 74.3, 85.2, and 92.4 eV, (ii) six resonances of ^{154}Gd at 22.3, 47.1, 49.5, 65.1, 100.7, and 124.0 eV, (iii) six resonances of ^{156}Gd at 33.2, 80.1, 150.4, 198.5, 341.0, and 376.7 eV, and (iv) seven resonances of ^{158}Gd at 22.3, 101.1, 242.7, 277.2, 344.8, 409.1, and 503.3 eV. These spectra or their averages for individual nuclei were used for further analysis.

There is a background in the MSC spectra constructed in this way, which arises from neutron capture on Ba in the detector and on the odd Gd isotopes in samples. This background was very small for strong resonances, see Fig. 2, and was subtracted. The shape of the background in the MSC spectrum for each multiplicity M was inferred from off-resonance regions. The absolute size was then obtained with the help of the sum-energy spectra for energies above the full-energy peak.

To facilitate the comparison of the data with model predictions, all sum-energy and MSC spectra for a given resonance were normalized such that the number of counts in

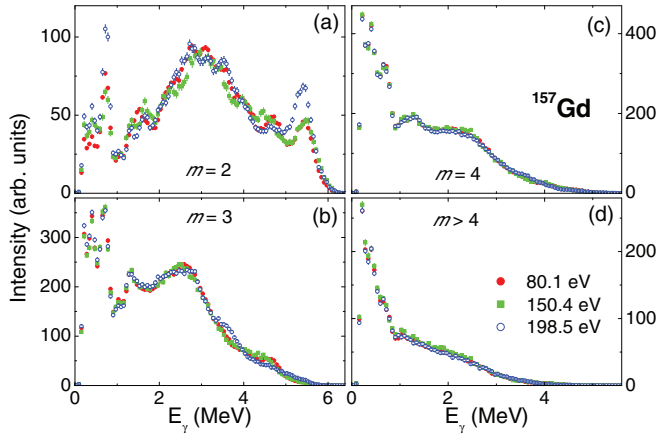

FIG. 3. (Color online) Experimental MSC spectra for three neutron resonances of ^{156}Gd target nucleus. Spectra for individual resonances were normalized as described the text.

the gray area in Fig. 1 is the same. In this way it was ensured that the integral of the sum-energy spectrum for multiplicities $m = 2$–7 in the $E_\Sigma^{(\mathrm{used})}$ range took a prefixed value common for all resonances. Only multiplicities $m = 2$–7 were used in the analysis. The spectrum for $m = 1$ is strongly dominated by background contributions and was omitted from the analysis. There are virtually no events for $m \geqslant 8$.

Experimental MSC spectra for three strong resonances in ^{156}Gd(n,γ) are shown in Fig. 3. The difference of MSC spectra in other isotopes is similar. As seen from the figure, the spectra from different resonances are very similar, especially for $M > 2$. They differ slightly from each other because of Porter-Thomas fluctuations of the primary γ-transition intensities [20]. This result also holds true for the other Gd isotopes.

For comparison with simulations the MSC spectra were prepared in the form of histograms with a bin width of 250 keV, comparable to the detector resolution. The use of these relatively wide bins facilitated the comparison between the experimental and simulated MSC spectra by suppressing the fluctuations without noticeably smearing the gross structures in these spectra.

III. SIMULATION OF MSC SPECTRA

The MCS spectra represent the main observables analyzed in this paper. As they are products of an interplay between level density and PSFs, they carry information on these quantities. Unfortunately, the interplay is quite complex and one cannot retrieve the PSFs and NLD directly from the MSC spectra. Therefore we adopted a trial-and-error approach in which we compared the experimental MCS spectra with the analogous spectra obtained from simulations under various assumptions about the shape and size of the NLD and PSFs. The degree of agreement between the experimental and simulated spectra allowed us to choose which of these models are most likely to be valid.

A. Algorithms

In each trial we proceeded as follows. Based on the statistical model, we simulated at random a γ cascade initiating at neutron capturing level with spin and parity $J^\pi = 1/2^+$ and determined subsequently the response of the DANCE array to this cascade.

Repeating these steps many times we mimicked an outcome of a fictitious experiment in which the product nucleus emits cascades governed by the postulated NLD and PSFs for a given trial. Then we followed the steps described in Sec. II B and accumulated a set of simulated MSC spectra under the same constraints as for the experimental MSC spectra.

The γ cascades were generated using the DICEBOX algorithm [21], while the response of the detector array was obtained from simulations of the detection process with the aid of GEANT4 code [22].

In the DICEBOX algorithm, below some critical energy, E_{crit}, all of the characteristics of the decay scheme of a product nucleus, i.e., the level energies, spins, and parities, as well as their decay pattern, are taken from existing experimental data. The choice of the critical energy was made with care to guarantee that the information for energies below E_{crit} is complete. The required data on low-lying levels for the isotopes of interest were taken from the ENSDF database [23–26]. The values of E_{crit} we adopted are listed in Table I.

Above E_{crit} the level system of the nucleus and its complete decay scheme are generated with the DICEBOX algorithm assuming the validity of an *a priori* chosen NLD function $\rho(E, J, \pi)$ and PSFs for multipolarities $E1$, $M1$, and $E2$. All higher multipolarities are neglected.

When generating transition intensities, a random partial radiation width $\Gamma_{a\gamma b}$ for a transition between an initial level a and a final level b is assumed to be

$$\Gamma_{a\gamma b} = \sum_{XL} \frac{\xi_{XL}^2 f^{(XL)}(E_\gamma, T) E_\gamma^{2L+1}}{\rho(E_a, J_a, \pi_a)}, \qquad (1)$$

where $f^{(XL)}$ stands for the photon strength functions for transitions of type X (electric or magnetic) and multipolarity L, and ξ_{XL} is a random number generated from a normal distribution with zero mean and unit variance. This random number ensures that the individual widths $\Gamma_{a\gamma b}$ fluctuate according to the PT distribution [20]. The argument T stands for nuclear temperature of the product nucleus exited at final level b. This argument is optional, as only some of the models considered in our analysis predict T-dependent PSFs. The sum in Eq. (1) is over all allowed types and multipolarities of transitions. Internal electron conversion, which is important in transitions between the lowest excited levels in Gd isotopes, is correctly treated throughout the simulations.

From the full set of partial radiation widths simulated according to Eq. (1) decay branching intensities, $I_{a\to b}$, for transitions from initial levels a to various levels b are calculated. The ratio $I_{a\to b} = \Gamma_{a\gamma b}/\Gamma_{a\gamma}$, where $\Gamma_{a\gamma} = \sum_{b'} \Gamma_{a\gamma b'}$ is the total radiation width of the initial level a.

Hereafter the simulated system of all levels, together with their branching intensities, is referred to as a nuclear realization. Due to PT fluctuations of partial widths $\Gamma_{a\gamma b}$, there

is an infinite number of nuclear realizations that differ from each other even for fixed models of PSFs and NLD. Therefore any predicted simulated observable is subject to an inherent, irreducible uncertainty originating from PT fluctuations of the partial radiation widths. In each trial we simulated 20 independent nuclear realizations for each of the PSF and NLD model combinations tested. Knowing all branching intensities and level energies, a large number of random γ cascades, in most cases 10^5, were generated separately for each nuclear realization. Each of the simulated cascades started at the neutron capturing level, which in our case was an isolated $J^\pi = 1/2^+$ neutron resonance.

As already mentioned, the cascade γ-ray energies are used as an input for the GEANT4-based simulation code to account for the detector response in order to construct the simulated MSC spectra. These MSC spectra, averaged over the nuclear realizations, together with the rms values of their inherent uncertainties were obtained and in the process of trial-and-error compared with their experimental counterparts. In addition, the total neutron radiation widths, which were obtained directly from DICEBOX simulations, were compared with the corresponding experimental values for individual target nuclei.

B. Photon strength functions

1. Electric-dipole transitions

It is well known that for γ-ray energies above S_n the electric-dipole ($E1$) transitions play a dominant role. The $E1$ PSF at these energies in axially deformed nuclei seems to be consistent with the sum of two Lorentzian terms

$$f^{(E1)}_{\rm SLO}(E_\gamma) = \frac{1}{3(\pi\hbar c)^2}\sum_{i=1}^{2}\frac{\sigma_{G_i}E_\gamma\Gamma^2_{G_i}}{\left(E^2_\gamma - E^2_{G_i}\right)^2 + E^2_\gamma\Gamma^2_{G_i}}. \quad (2)$$

Here E_{G_i}, Γ_{G_i}, and σ_{G_i} are the parameters of the giant electric dipole resonance (GEDR), which is split into two components ($i = 1$ and 2) in axially deformed nuclei. The model given by Eq. (2) is known as the Brink-Axel or standard Lorentzian (SLO) model [27].

The SLO model describes the data from photonuclear reactions very well. Unfortunately, the values of its parameters E_{G_i}, Γ_{G_i}, and σ_{G_i} obtained from these data are not available for the Gd nuclei of our interest. For this reason, in our simulations we relied on values of E_{G_i}, Γ_{G_i}, and σ_{G_i} obtained from (γ, n) reactions on the nearby nuclei ^{154}Sm and ^{160}Gd [28]. This seems to be justified, as these parameters are expected to vary smoothly with A. In addition, the (γ, n) data do not display any pronounced odd-even A effect. In our case, the fit of $f^{(E1)}$ from (γ, n) data on ^{154}Sm and ^{160}Gd is almost indistinguishable at γ-ray energies below about 9 MeV. As for the interpretation of the main observables—the sum-energy, the MCS spectra, and the total resonance radiation width—our primary interest was the sizes and shapes of $f^{(E1)}$ at $E_\gamma < S_n$.

Although there is essential agreement on the energy dependence of the giant resonance at energies accessible from (γ, n) experiments, the shape of the $E1$ PSF below the neutron separation energy S_n is not well known. There are many available parametrizations of the $E1$ PSF in this region of γ-ray energies that modify the Lorentzian shape of the low-energy tail of the GEDR. Usually one of two models is used. The first one was proposed by Kadmenskij, Markushev, and Furman [29] for the description of the $E1$ PSF at low E_γ in spherical or weakly deformed nuclei and is known as the KMF model. Although there is no justification for the applicability of this model to well-deformed nuclei, it is often adopted for these nuclei.

A second widely used model was proposed for spherical nuclei by Chrien [30] in order to match the behavior of the SLO model at energies near the GEDR maximum and the KMF model at very low E_γ. This phenomenological model was later generalized for deformed nuclei by Kopecky *et al.* [31] by introducing an *ad hoc* parameter k. The systematics of this parameter in Ref. [27] was based on the requirement to reproduce the total neutron radiation widths. Since the width strongly depends on the NLD model below S_n, as well as the PSFs for other multipolarities, we considered the parameter k to be a free parameter in our simulations. This model is known as the enhanced generalized Lorentzian (EGLO) model. The model, as introduced in Ref. [31], is

$$f^{(E1)}_{\rm EGLO}(E_\gamma, T) = \sum_{i=1}^{2}\frac{\sigma_{G_i}\Gamma_{G_i}}{3(\pi\hbar c)^2}\left[\mathcal{A}(E_\gamma, T) + \frac{F_K\Gamma_{G_i}(E_\gamma = 0, T)}{E^3_{G_i}}\right], \quad (3)$$

$$\mathcal{A}(E_\gamma, T) = \frac{E_\gamma\,\Gamma_{G_i}(E_\gamma,\,T)}{\left(E^2_\gamma - E^2_{G_i}\right)^2 + E^2_\gamma\,\Gamma^2_{G_i}(E_\gamma,\,T)}. \quad (4)$$

Here, the factor $F_K = 0.7$ [29,32], and the temperature-dependent width $\Gamma(E_\gamma, T)$ is given by

$$\Gamma_{G_i}(E_\gamma, T) = \Gamma_{G_i}\frac{E^2_\gamma + 4\pi^2T^2}{E^2_{G_i}}\left[k + (1-k)\frac{E_\gamma - E^0_\gamma}{E_{G_i} - E^0_\gamma}\right], \quad (5)$$

with the temperature $T = T(E) \equiv \sqrt{(E-\Delta)/a}$; E is the excitation energy of a final level, $E^0_\gamma = 4.5$ MeV [31], a the shell-model NLD parameter and Δ the pairing energy. The values of a were adopted from Refs. [33,34]. The values of Δ were then obtained according to the formula for proton pairing in Ref. [35]—it was assumed that there is no neutron pairing in odd nuclei. Our results are insensitive to a change of Δ of up to at least 200 keV.

The EGLO model, which was tested in our previous Gd measurements [4,5] differed from the original model in the second term on the right-hand side of Eq. (3), which describes the behavior of the model at very low γ-ray energies. Specifically, the model, which will be denoted as the modified generalized Lorentzian (MGLO) in the following, assumed that $k \equiv 1$ in this second term of Eq. (3), so that the expression for the MGLO $E1$ PSF reads

$$f^{(E1)}_{\rm MGLO}(E_\gamma, T) = \sum_{i=1}^{2}\frac{\sigma_{G_i}\Gamma_{G_i}}{3(\pi\hbar c)^2}\left[\mathcal{A}(E_\gamma, T) + \frac{4\pi^2\,F_K\,\Gamma_{G_i}\,T^2}{E^5_{G_i}}\right]. \quad (6)$$

The MGLO model is similar to the KMF one for $k \sim 2$. For the EGLO and MGLO models we decided to fix the parameter E_γ^0, but to let the parameter k vary in the simulations.

In addition, many other models of the $E1$ PSF can be found in the literature. The RIPL-3 database [27]—probably the database most widely used by experimentalists—lists several additional closed-form models. These include the so-called hybrid model (GH) [36], the generalized Fermi liquid (GFL) model [37], and a family of modified Lorentzian (MLO) models; there are at least three different MLO models in the database. For a comprehensive description of all these models, the reader is referred to Ref. [27]. Further, a PSF model originating from Hartree-Fock-Bogoljubov (HFB) calculations is in RIPL-3. All of these models have been tested in our analysis. Many of them use values of E_{G_i}, Γ_{G_i}, and σ_{G_i} as parameters. The same values of these parameters as in the SLO model were adopted in all models considered.

For a complete description of γ decay one needs information on the PSFs at all excitation energies. In some models, the dependence on any quantity other than E_γ is neglected. This assumption is known as the Brink hypothesis [38], which was formulated for $E1$ transitions originating from the fragmentation of the GEDR. Experimental data from average resonance capture [39] and from ^{3}He-induced reaction [15] seem to confirm at least the approximate validity of the hypothesis in the region of excitation energies below S_n.

From the above list of closed-form models for $E1$ PSF, only the SLO model is assumed to follow the strict form of the Brink hypothesis. In addition, the hypothesis must be invoked for the description of transitions between excited states in combination with the $E1$ PSF from HFB calculations. The remaining models predict a weak dependence of the PSF on the nuclear temperature T.

The γ-ray energy dependence of the PSFs for several of the models considered is shown in Fig. 4. There are two curves for the KMF, MGLO, and MLO models of $E1$ PSF shown. They indicate how these models change as a function of temperature—the lower curve corresponds to $T = 0$ while the upper one to $T = \sqrt{(S_n - E_\gamma - \Delta)/a}$. To keep the figure readable we only display a representative sample of the models.

In addition to the models listed above, a modification of the KMF model, which satisfies the Brink hypothesis, a KMF model with fixed temperature T (KMF-T model), is sometimes used. This is especially true in the analysis of data measured with the Oslo method [15,40], which relies on the validity of the Brink hypothesis. During analysis of MSC spectra in ^{156}Gd we found that simulations with this model reproduce experimental spectra for $T = 0.3 - 0.35$ MeV [5]. This value of T is in very good agreement with the value obtained from Oslo measurements in deformed nuclei, usually $T \approx 0.3$ [14,15].

2. *Magnetic-dipole transitions*

Magnetic-dipole ($M1$) transitions also play an important role in the decay of highly excited nuclear states below S_n. In the mid 1970s, Hilton [6] and later Lo Iudice and Palumbo [7], using the geometrical two rigid rotors model, and Iachello [41],

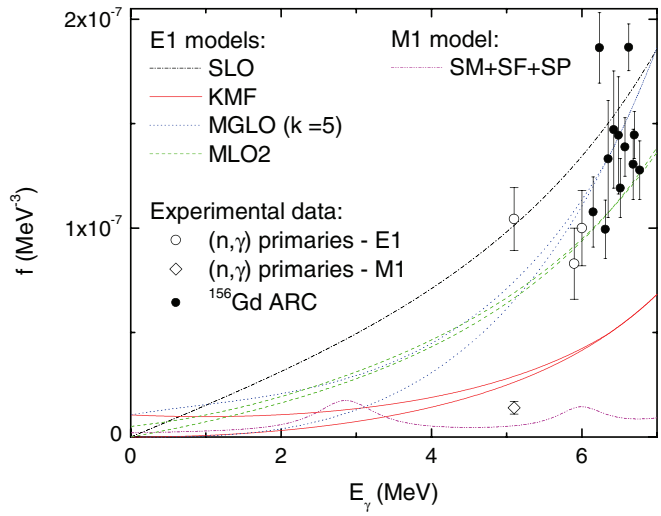

FIG. 4. (Color online) Energy dependence of SLO, KMF, MGLO ($k = 5$), MLO2 $E1$ PSFs models together with the composite $f^{M1} = f^{M1}_{\rm SM} + f^{M1}_{\rm SF} + f^{M1}_{\rm SP}$ model. For more detailed description see Secs. III B 1 and III B 2. The experimental data for $f^{(E1)}$ and $f^{(M1)}$ in ^{155,157,159}Gd, at energies 5.9, 6.0 and 5.1 MeV, respectively, are from the RIPL database [32] (^{155,157}Gd) and Ref. [42] ^{159}Gd. Data from average resonance capture (ARC) in ^{155}Gd are from Ref. [37].

using the proton-neutron interacting boson model, predicted an isovector $M1$ collective vibrational mode in deformed nuclei. This mode, known as the scissors mode, was initially observed for ground-state transitions in ^{156}Gd by Bohle *et al.* [8] via high-resolution electron inelastic scattering at low momentum transfer.

A systematic study of ground-state transitions for $E_\gamma \lesssim 4$ MeV in even-even rare-earth nuclei was performed with the (γ,γ') reaction [9]. The low density of $J = 1$ states (average spacing of several tens of keV) allows observation of a majority of the dipole transition strength at these energies. In these experiments the total observed $M1$ strength in the energy range $E_\gamma \approx 2.5$–4.0 MeV in even-even rare-earth nuclei is fragmented into several transitions and is proportional to the square of the nuclear deformation [10]. For well-deformed nuclei the strength reaches $\sum B(M1)\uparrow \approx 3\mu_N^2$. All of the $M1$ strength in this energy range is usually ascribed to the SM. The centroid of the SM strength is located near 3 MeV and is almost independent of A in rare-earth nuclei [43].

The spacing between the levels near 3 MeV in odd nuclei is of the order of keV, which is too small to resolve all transitions populating these levels from the ground state. If fragmentation of the SM strength follows the Porter-Thomas distribution, a significant fraction of the strength has to be carried by many weak transitions, which may not be detected. Therefore the SM strength determined for odd nuclei from (γ, γ') reaction is underestimated. This seems to be documented by NRF experimental data—a significantly smaller total $M1$ strength is observed for odd nuclei compared to neighboring even-even nuclei [44–46]. For example, data for two odd Gd isotopes yield $\sum B(M1)\uparrow = 0.34$ and $1.02\ \mu_N^2$ for ^{155}Gd and ^{157}Gd, respectively. This values are much lower than those for neighboring even-even nuclei [9].

Furthermore, as the type and multipolarity of the observed transitions in odd nuclei cannot be easily determined in (γ, γ') experiments, the strength carried by the observed transitions from the ground state to the 3 MeV region may include a contribution from $E1$ transitions. Usually all of the strength observed in (γ,γ') experiments on odd nuclei is attributed to the SM contribution.

Attempts to estimate the missing strength in (γ, γ') reactions were made. The aim was to reconcile the data on the full $M1$ strength for odd nuclei with those for even-even nuclei. For this purpose a fluctuation analysis of the γ-ray spectra was developed [46,47]. However, for ^{163}Dy this type of analysis does not work properly [44]. Thus, the fluctuation-based corrections of the NRF data for missing strength in the remaining odd nuclei studied seem questionable.

Later, the analysis of data on TSCs following thermal neutron capture in ^{162}Dy suggested that a resonancelike structure of $M1$ character and equal strength couples not only to the ground state, but also to all levels in ^{163}Dy [11]. It is thus natural to assume that the SM obeys the Brink hypothesis. A similar finding was corroborated by the behavior of MSC γ-ray spectra obtained from isolated resonances of odd Gd nuclei [4,5] and also by data on ^{3}He-induced photon production [13].

The analysis of TSC spectra in Ref. [11] indicated that the reduced SM strength in odd ^{163}Dy is higher compared to that deduced from (γ, γ') measurements on neighboring even-even nuclei. The total SM strength reported in Ref. [11] is $\sum B(M1)\uparrow \approx 6.2\mu_N^2$. Comparable strength of the scissors mode in odd and even-even nuclei was reported from ^{3}He-induced reactions on Dy nuclei [15,40]. Interestingly, data from the same reaction yielded about 1.7 times higher strength of the SM in odd ^{167}Er than in even-even ^{166}Er [48]. The total strength reported in Ref. [15] is $\approx 6-7\mu_N^2$ for all Dy nuclei. However, the SM strength deduced from ^{3}He-induced reactions depends strongly on the assumed shape of the $E1$ PSF and may be significantly smaller, see the discussion in Sec. V.

The data from (n, γ) and ^{3}He-induced reactions indicate that the SM is pronounced in the $M1$ PSF as a resonance-like component with a half width of $\approx 0.7-1.5$ MeV. The maximum of the resonance structure is close to 3 MeV in the (n, γ) reaction, while it is slightly shifted down—to about 2.7–2.8 MeV—in data from the latter reactions.

Our recent analysis of MSC spectra from resonance neutron capture in the odd ^{155,157}Gd isotopes indicated [4,5] that the strength of the SM in even Gd nuclei is slightly smaller than the total $M1$ strength observed for ground-state transitions from the (γ,γ'). In addition, a nonresonant part of $M1$ strength $f_{\rm SP}^{(M1)}$ must be added to the SM in order to reproduce experimental MSC spectra. It was also observed that the parameters of the SM determined from studies of ^{3}He-induced reactions in neighboring even-even Dy isotopes [14,15,40] were not consistent with our data on even-even Gd isotopes.

The $M1$ strength is more complex than just the contribution of the SM. Usually, one of two models is used for the remaining part of the $M1$ strength. In the spin-flip (SF) resonance model, $f_{\rm SF}^{(M1)}(E_\gamma)$, it is often assumed that the resonance has a Lorentzian shape with an energy of about 7 MeV and a width of 4 MeV [27], while in the single-particle (SP) model, $f_{\rm SP}^{(M1)}$ is a constant independent of γ-ray energy. The $M1$ strength corresponding to the spin-flip mode was obtained from inelastic proton scattering on several even-even rare-earth nuclei [49]. A double-humped structure was observed between 5 and 10 MeV and we adopted this form of the SF resonance in our simulations. The Lorentzian shape was assumed for both resonance components. In some cases a sum of the strengths from the two models, $f_{\rm SP}^{(M1)}$ and $f_{\rm SF}^{(M1)}$, is used for the $M1$ PSF. In our earlier analysis of MSC spectra in even-even Gd isotopes [4,5] we were only able to reach a reasonable agreement between the simulations and experiment with a composite model for $M1$ strength: $f^{(M1)} = f_{\rm SM}^{(M1)} + f_{\rm SF}^{(M1)} + f_{\rm SP}^{(M1)}$ with $f_{\rm SP}^{(M1)} \approx (1-2.5)\times 10^{-9}$ MeV^{-3}.

In our simulations the SM was always represented with a single Lorentzian resonance term and the search for the SM parameters was the main focus of this work. The absolute values of the SP and SF models were adjusted to obtain the ratio of $R = f^{(E1)}/f^{(M1)} \approx 7$ at 7 MeV. This value seems to be reasonably well determined in rare-earth nuclei from average resonance capture experiments [39]. In models adopting the sum of SP and SF contributions, we varied $f_{\rm SP}^{(M1)}$ and adjusted the size of the SF contribution to reproduce the ratio R. The strict validity of the Brink hypothesis was assumed for SP and SF $M1$ models.

The γ-ray energy dependence of an $M1$ PSF, given by the sum of SP, SF, and SM contributions, is shown in Fig. 4. The parameters of the scissors mode were $E_{\rm SM} = 2.9$ MeV, $\Gamma_{\rm SM} = 1.0$ MeV, and $\sigma_{\rm SM} = 0.5$ mb. The SP strength was adjusted to $f_{\rm SP}^{(M1)} = 2\times 10^{-9}$ MeV^{-3} and the size of the SF contribution was adjusted to obtain the ratio $R \approx 7$ at 7 MeV with respect to the KMF model for $E1$ PSF.

3. *Electric-quadrupole transitions*

In addition to dipole transitions, electric quadrupole ($E2$) transitions might also play a role in neutron resonance decay. We found that $E2$ transitions are not important in the interpretation of our data; we adopted a simple single-particle model ($f_{\rm SP}^{(E2)} = $ const.) in our simulations. The strength of $f_{\rm SP}^{(E2)}$ was taken to reproduce the ratio of partial radiation widths at about 7 MeV measured in average resonance capture experiments in even-even deformed nuclei, which is $\Gamma(E1)/\Gamma(E2) \gtrsim 100$ [39].

C. Nuclear level density

There are many NLD models in the literature. We tested three different models for the energy dependence of the NLD. Two of them were given by closed-form formulas: (i) the back-shifted Fermi gas (BSFG), and (ii) the constant-temperature (CT) model [33]. There are two adjustable parameters in each of these models. Two different parameter sets were tested for each of these NLD models; they were taken from von Egidy and Bucurescu [33,34]. The spin dependence of the NLD for

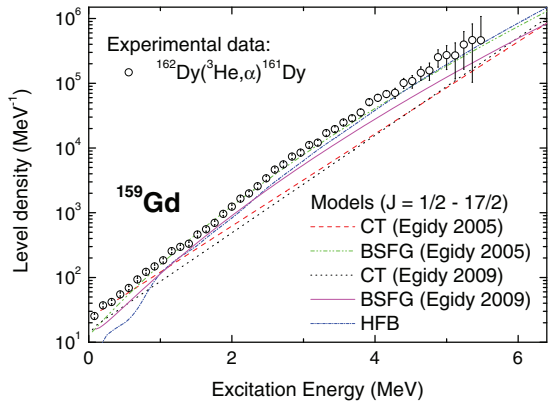

FIG. 5. (Color online) Spin- and parity-summed level density function for ^{159}Gd according to CT and BSFG models and HFB calculations. The parameters of the CT and BSFG NLDs were adjusted following two parametrizations according to Refs. [33,34]. For comparison, the experimental data from Ref. [14] on the NLD for ^{161}Dy are also plotted. Different predicted absolute values at $S_n = 5.94$ MeV originate from the different spin distributions in the models. The resonance spacing of s-wave resonances [27] is the same in all models.

both of the models was adopted in the standard form [27,33,34]; no parity dependence was assumed above $E_{\rm crit}$.

In addition to these closed-form models, we also tested the NLD calculated within the Hartree-Fock-Bogoljubov (HFB) approach. This density is available in tabulated form as a function of energy for levels with each spin and both parities [27,50].

In order to bring the calculations into agreement with experimental data, the HFB level density was multiplied by a constant factor to reproduce the spacing of s-wave neutron resonances. Even after this absolute renormalization, the model may fail to reproduce the number of levels at very low excitation energies—this happened for ^{157,159}Gd. In this case, additional renormalization of the energy dependence of the HFB NLD model must be applied [27].

All known levels below $E_{\rm crit}$ are taken into account in the simulations. The level density formula is thus applied only above this energy. There are NLDs inferred from ^{3}He-induced measurements in neighboring odd Dy isotopes [14,15]. The energy dependence of NLD in ^{161}Dy seems to be much closer to that given by the BSFG model than by the CT model, see Fig. 5.

IV. RESULTS FROM MSC SPECTRA

Several hundred model combinations of PSFs and NLD functions were used in simulations for each Gd isotope. To quantify the degree of agreement between the simulated and experimental MSC spectra, extremely time-consuming simulations would be needed as contents of individual bins in MSC spectra are mutually correlated in a complicated fashion and the corresponding correlation matrix is not known *a priori*. As a consequence, the degree of agreement was only checked visually. Proper quantitative characterization of the degree of the agreement would require simulations of an extremely large number of nuclear realizations.

To characterize uncertainties due to Porter-Thomas and NLD fluctuations we do not plot a set of spectra calculated for individual realizations, but only the standard confidence region of spectral intensity, characterizing the behavior of this set. This confidence region is plotted in Figs. 7–11 in form of a gray band; each band has a width of two sigma (the average ± one sigma) with the mean and sigma taken from the 20 nuclear realizations. The size of fluctuations among the experimental spectra for different resonances is reasonably well reproduced by the simulations.

We should stress that within the enormous domain of PSFs and NLD functions the adopted trial-and-error method does not guarantee finding a model and its parameters yielding the best agreement between simulated and experimental MSC spectra. Nevertheless, we did find several combinations of PSFs and NLD function, which lead to reproduction of the experimental spectra, see below.

As an influence of the $E2$ PSF on the shape of simulated MSC spectra is negligible, we restrict the discussion only on the NLD, $E1$ and $M1$ PSFs.

A. Nuclear level density

With the CT model for the NLD, we found that for any of Gd isotopes studied none of the tested combinations of PSFs yielded an acceptable prediction of the MSC spectra. On the other hand, for all of the nuclei studied we were able to find several PSFs models, see below, which reproduce the data in combination with the BSFG model.

A slightly better agreement with experimental MSC spectra is obtained with the older parametrization of the model [33]. The new parametrization [34] cannot be ruled out, which illustrates the limited sensitivity of our analysis to the spin dependence of the NLD. The difference in the spin distribution can be seen from Fig. 5—the total level density near S_n is rather different in the two BSFG parametrizations despite the fact that the spacing of s-wave resonances is the same. Using the calculations based on the HFB approach for NLD in our simulations of the MSC spectra for ^{153}Gd and ^{155}Gd we reached an acceptable agreement with experiment. For two heavier isotopes ^{157,159}Gd the agreement is not as good as with the BSFG model even if a renormalization of the energy dependence was applied to this model. However, we cannot completely rule out this model for any of the isotopes studied.

B. Electric dipole PSF

An acceptable agreement between simulated and experimental MSC spectra was obtained with several models of the $E1$ PSF. Specifically, for all nuclei a reasonable reproduction of the MSC spectra was obtained with the KMF, KMF-T, GH, MLO1, MGLO, and SLO models.

In the case of the MGLO model, the range of optimum values of the parameter k in simulations for ^{153,155}Gd was found to be $k \approx 1.5$–3.0, while for ^{157,159}Gd we needed $k \approx 2.5$–5.5. With the KMF-T model agreement was achieved with

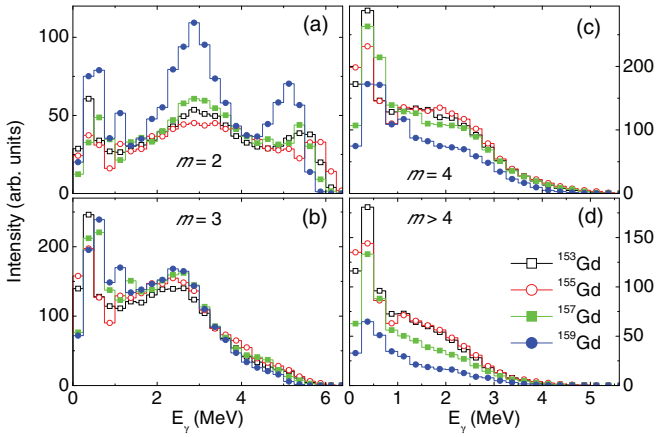

FIG. 6. (Color online) A comparison between averaged experimental MSC spectra for ^{153,155,157,159}Gd plotted separately for cluster multiplicities $m = 2, 3, 4$, and > 4. For each nucleus, the averaging was over the full set of strong $J^{\pi} = 1/2^{+}$ resonances with energies specified in Sec. II B. For convenience, the MSC intensities were rescaled to ensure that the sum of areas under the MSC spectra over all m is the same for all four nuclei.

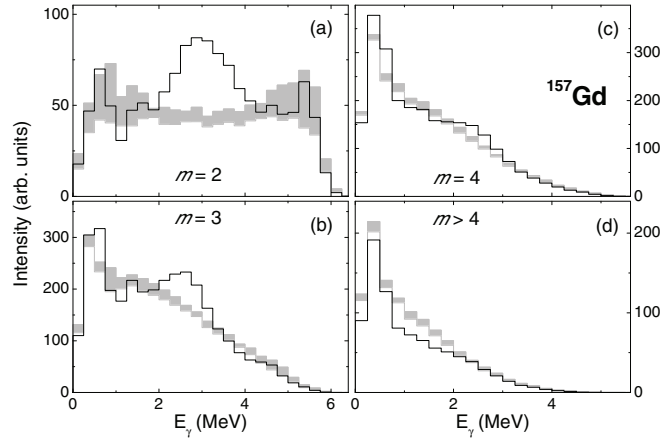

FIG. 7. A comparison between the averaged experimental MSC spectra for ^{157}Gd (solid line) and the simulated spectra for cluster multiplicities $m = 2, 3, 4$, and > 4. The simulations assumed the BSFG model for the NLD, the KMF model for the $E1$ PSF, and the SF model for the $M1$ PSF, neglecting any resonancelike structure at $E_{\gamma} \approx 3$ MeV in a PSF. The simulated MSC intensities and their uncertainties are represented by gray areas, see the main text. The relative uncertainties of the experimental MSC intensities are less than 2%.

a temperature of $T = 0.25$–0.40 MeV. For the ^{157,159}Gd nuclei, an acceptable agreement between simulations and data was also reached with the MLO2 and MLO3 models. On the other hand, the simulations that relied on the GFL, EGLO, and HFB-based models were found to be in sharp disagreement with the experimental MSC spectra. In addition, as will be apparent from further discussion in Sec. V, it is very unlikely that the SLO model is valid.

Our analysis did not allow us to make a unique choice out of the above-listed acceptable models for the $E1$ PSF. As discussed below, this is at least partly an artifact of the strong role of SM $M1$ strength at $E_{\gamma} \approx 3$ MeV. This drawback did not allow us to say much about the $E1$ PSF, but did give us more confidence in the parameters determined for the SM. The limited sensitivity of our experiments to the $E1$ strength prevented us from confirming or rejecting the need for the temperature dependence of the $E1$ PSF.

C. Magnetic dipole PSF

The MSC spectra for all isotopes have similar shapes. Specifically, there is a pronounced bump in the middle of the $M = 2$ spectra. A distinct bump is also present between 2 and 3 MeV in the $M = 3$ spectra. As the mass of the nucleus increases, the bump in the $M = 2$ spectrum becomes more pronounced and at the same time the intensity of the spectrum for $M > 3$ becomes weaker, which is apparent from Fig. 6.

The presence of this bump indicates that a PSF includes a resonancelike component with a maximum near 3 MeV. Without postulating such a component our simulations could not reproduce the bump in the experimental MSC spectra, see the example shown in Fig. 7.

Further, comparison of simulations with experimental MSC spectra clearly shows that the resonance enhancement near 3 MeV of the postulated photon strength does not lead to a good agreement if it is attributed purely to $E1$ transitions. This is documented for the case of ^{157}Gd in Fig. 8. A similar disagreement was found for all remaining nuclei. We note that the sensitivity of the MSC spectra to the multipolarity responsible for the bump in MSC spectra is substantiated by the fact that the parity of s-wave resonances is opposite to that of the ground state for each of odd Gd nuclei.

We can not unambiguously distinguish between the $M1$ and $E2$ character of that part of the resonance enhancement responsible for the bump in the MSC spectra. This is because the sensitivity of these spectra to both multipolarities is very

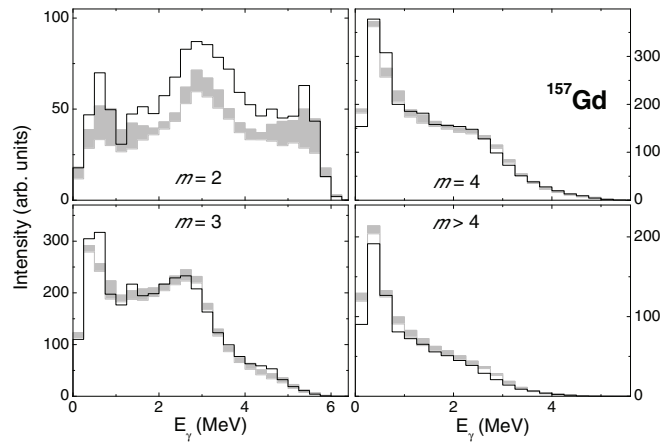

FIG. 8. A comparison between the averaged experimental MSC spectra for ^{157}Gd (solid line) and the simulated spectra. The simulations were performed assuming the BSFG model for the NLD, and the SF model for the $M1$ PSF. For the $E1$ PSF a combination of the KMF model and a Lorentzian resonance structure postulated at 3 MeV was used. For other details see the caption of Fig. 7.

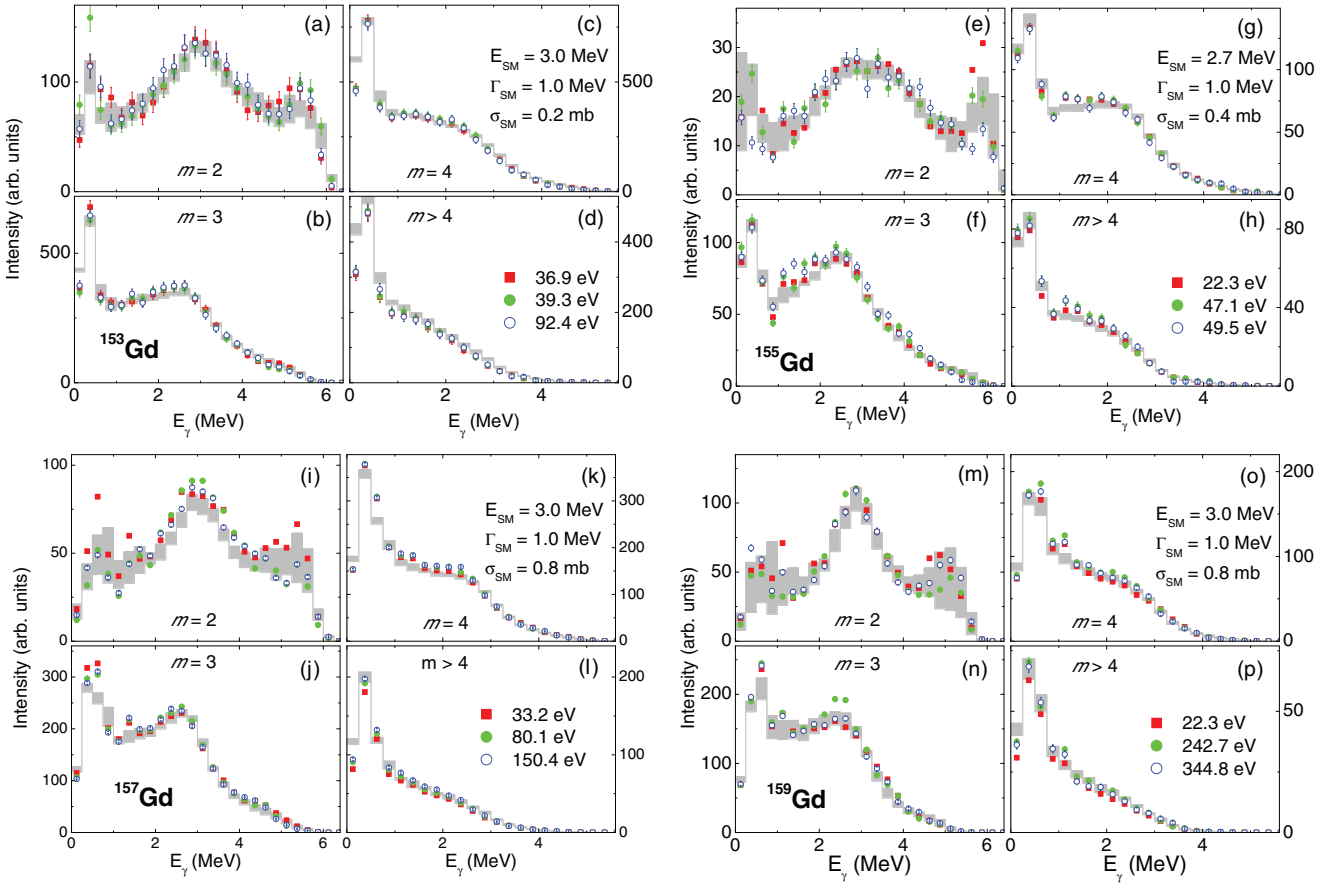

FIG. 9. (Color online) A comparison between experimental MSC spectra determined from several neutron resonances of ^{152,154,156,158}Gd$(n,\gamma)^{153,155,157,159}$Gd reactions (symbols) with MSC spectra from simulations (gray area) displaying the best agreement with experiments. The simulations were performed with the BSFG model for NLD and MGLO model for $E1$ PSF with $k = 2$, 3, 4, and 4 assumed for ^{153,155,157,159}Gd, respectively. For $M1$ PSF, a composite model $f^{M1} = f^{M1}_{\rm SM} + f^{M1}_{\rm SF} + f^{M1}_{\rm SP}$; $f^{M1}_{\rm SP} = 2 \times 10^{-9}$ MeV^{-3}. The SM parameters as well as the energies of neutron resonances for each product nucleus are indicated.

similar, due to the same parity selection rules for $M1$ and $E2$ transitions. Nevertheless, we interpret the bump as an artifact of a resonancelike component of the $M1$ PSF. This interpretation is corroborated by the enhanced $M1$ ground-state transitions observed near 3 MeV in (γ,γ') reactions on deformed nuclei.

Adding a Lorentzian term into the $M1$ PSF the simulations led to excellent agreement between the experimental and simulated MSC spectra. This agreement was achieved for all odd Gd nuclei studied and for several $E1$ PSF models, see above. This is illustrated for the MGLO model in Fig. 9.

In an attempt to find the best agreement between simulations and experiment, we proceeded as follows. (i) We selected one of the models for the $E1$ PSF and NLD and kept these models common to all four Gd isotopes studied. (ii) We performed separate simulations of the MSC spectra for individual isotopes for various combinations of values of SP $M1$ PSF and SM parameters. (iii) Finally, we estimated values of these parameters which provided the best agreement. Steps (i)–(ii) were repeatedly performed using all of the $E1$ PSF and NLD models listed in Sec. III. With this approach we found the best parameter estimates for $E_{\rm SM}$ (the centroid energy of the SM), $\Gamma_{\rm SM}$ (the width of the SM), $\sigma_{\rm SM}$ (the maximum SM cross section), and $f^{(M1)}_{\rm SP}$ for each choice of fixed $E1$ PSF and NLD models. Naturally, these estimates differed from each other for different $E1$ PSF models, but their variation was not very large, which is documented in Table II, where the ranges of parameter estimates are listed. The values in the Table II correspond to the minimum and maximum acceptable values and their ranges include uncertainties due to our inability to decide which of the $E1$ PSF models is closer to the actual photon strength.

We stress that in each simulation trial the Lorentzian SM parameters were independent of excitation energy. In the spirit of the Brink hypothesis, this agreement suggests that the SM affects not only the ground-state transitions, as seen from (γ,γ') data, but also transitions to any exited nuclear level.

To examine this further, we undertook simulations assuming that the SM is coupled only to the levels with energies below certain excitation energy $E_{\rm max}$. The result for ^{157}Gd and $E_{\rm max} = 3$ MeV is displayed in Fig. 10. Rejection of this option can be made with high confidence for all of the nuclei studied and for $E_{\rm max} \lesssim 4$–5 MeV. In practice, for higher values of $E_{\rm max}$ we lose sensitivity as SM resonances built on levels above 4 or 5 MeV do not influence the decay following the resonance

TABLE II. Minimum and maximum acceptable values of the SM parameters obtained from the analysis considering the KMF, KMF-T, GH, MGLO, and MLO models of $E1$ PSF. For the SLO model the value of σ_{SM} would be much higher, see the text for discussion of this model. Values for the even-even Gd isotopes, published in Refs. [4,5], are included. The meaning of the individual values of reduced transition probability $\sum B(M1)\uparrow$ is explained in Sec. V D. Theoretical nuclear deformation parameters β_2 for studied Gd nuclei are taken from Refs. [53,54].

Product	E_{SM}	Γ_{SM}	σ_{SM}	$\Sigma B_{NRF}(M1)\uparrow$	$\Sigma B_{NRF}(SP+SF)\uparrow$	$\Sigma B_{tot}(SM)\uparrow$	β_2	
	(MeV)	(MeV)	(mb)	μ_N^2	μ_N^2	μ_N^2	[53]	[54]
^{153}Gd	2.8–3.0	0.9–1.3	0.2–0.25	1.7–2.3	0.3(2)	2.1–3.4	0.320	0.215
^{155}Gd	2.5–2.7	1.0–1.2	0.2–0.4	1.8–3.4	0.6(1)	2.5–5.8	0.340	0.252
^{156}Gd	2.7–3.1	0.8–1.4	0.07–0.32	1.6–2.5	0.5(2)	1.9–3.5	0.330	0.271
^{157}Gd	3.0–3.1	0.8–1.2	0.6–1.0	4.0–6.1	0.1(1)	6.5–9.6	0.360	0.271
^{158}Gd	2.8–3.1	0.6–1.6	0.07–0.25	1.3–2.2	0.5(1)	1.4–2.8	0.340	0.271
^{159}Gd	2.9–3.1	0.8–1.1	0.6–1.0	3.9–6.2	0.1(1)	6.9–10.9	0.360	0.280

neutron capture. We also tried linear increase or decrease of parameters E_{SM}, Γ_{SM}, and σ_{SM} with excitation energy. The results indicated that all of these parameters are very stable, i.e., they do not vary significantly with excitation energy.

For ^{153,157,159}Gd nuclei our values for the SM energy, E_{SM}, are very close to 3 MeV, see Table II. However, for ^{155}Gd nucleus this energy is apparently shifted towards lower values. We have no explanation for this finding. The damping width of the SM is in all cases very close to 1 MeV. As expected, estimates of the parameters E_{SM} and Γ_{SM} from simulations were found to be insensitive to the postulated $E1$ PSF.

On the other hand, estimates of σ_{SM} differ more significantly from each other for various considered $E1$ PSF models. Referring to Table II, this sensitivity is reflected by a relatively broad range of estimates of σ_{SM}. As an example, the $E1$ PSF values predicted by the MGLO model with $k = 5$ are significantly higher compared to those corresponding to the KMF or GH models in the SM energy region, see Fig. 4.

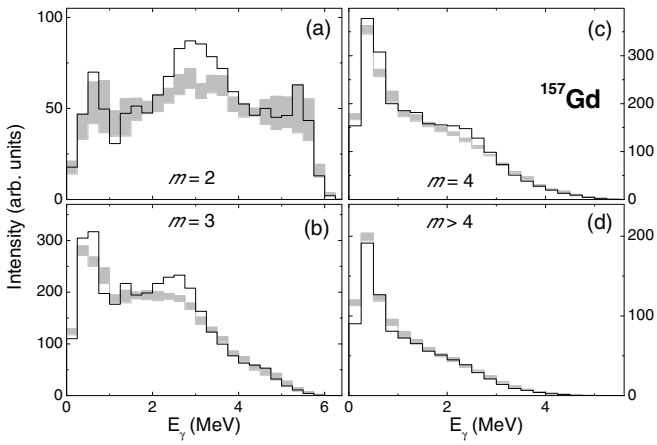

FIG. 10. A comparison between the averaged experimental MSC spectra for ^{157}Gd and the simulated spectra. The KMF model was adopted for the $E1$ PSF, while BSFG model for the NLD. For $M1$ PSF a model, the $f_{SF}^{(M1)} + f_{SP}^{(M1)}$ component was assumed to follow the Brink hypothesis while the SM resonance structure centered at 3 MeV and with strength of 7.2 μ_N^2 was considered only on levels up to 3 MeV of excitation energy. The SM resonance in $M1$ PSF was completely absent for transitions to higher excitation energies. For details see the caption of Fig. 7.

Consequently, in order to reproduce the bumps in $M = 2$ and 3 in the experimental MSC spectra, higher values of σ_{SM} are needed for the MGLO model as compared to those for the KMF model. The sensitivity of σ_{SM} to the postulated $E1$ strength is indeed observed: the values of σ_{SM} based on the validity of the KMF or GH models are close to the lower limits for this quantity, while the values for the MLO or MGLO models with $k \approx 3$–5 are near the upper limits from Table II.

In the SM γ-ray energy region the values of the $E1$ PSF according to the SLO model are significantly higher than the values predicted by the remaining $E1$ models, see Fig. 4. To mimic the 3 MeV bump in experimental MSC spectra assuming this $E1$ PSF model, values of $\sigma_{SM} = 0.6$–0.8 mb and $\sigma_{SM} = 1.6$–2.0 mb would be required for ^{153,155}Gd and ^{157,159}Gd, respectively. These values are a factor of three higher compared to what we obtained from simulations relying on the other $E1$ PSF models. As shown in Sec. V, it is highly unlikely that the SLO model can be a reasonable description of the $E1$ PSF due to huge problems with the total radiative width predicted by this model.

As mentioned in Sec. III B 2, in order to reproduce the MSC spectra in even-even Gd isotopes [4,5] we needed to use a composite model for the $M1$ strength: $f^{(M1)} = f_{SM}^{(M1)} + f_{SF}^{(M1)} + f_{SP}^{(M1)}$. The odd Gd nuclei are sensitive to the $f_{SP}^{(M1)}$ part of the $M1$ PSF. Adding $f_{SP}^{(M1)}$ with the strength needed in even-even nuclei, $f_{SP}^{(M1)} \approx (1$–$2.5) \times 10^{-9}$ MeV^{-3}, improves the agreement between simulated and experimental MSC spectra in ^{153,155}Gd, but it does not significantly change the agreement in ^{157,159}Gd. If a larger $f_{SP}^{(M1)}$ is used, the agreement with experiment is worse. There is virtually no sensitivity to the parameters of the SF mode used in simulations.

In spite of difficulties in determining the $E1$ photon strength, we could still make several firm conclusions. Our analysis indicated that values of σ_{SM} for ^{157,159}Gd are higher, by a factor of $\approx$3, compared to ^{153,155}Gd. Although estimates of σ_{SM} vary with the choice of an $E1$ PSF model, there is a marked difference between the values of σ_{SM} for heavier and lighter Gd nuclei, which persists with a fixed $E1$ PSF model. The significance of this difference is apparent in Fig. 11 for ^{157}Gd. It is clear that the estimated value of σ_{SM} from ^{153,155}Gd data, and also from even ^{156,158}Gd data [4,5] is too low to account for the bump at 3 MeV at the MSC spectra for ^{157}Gd.

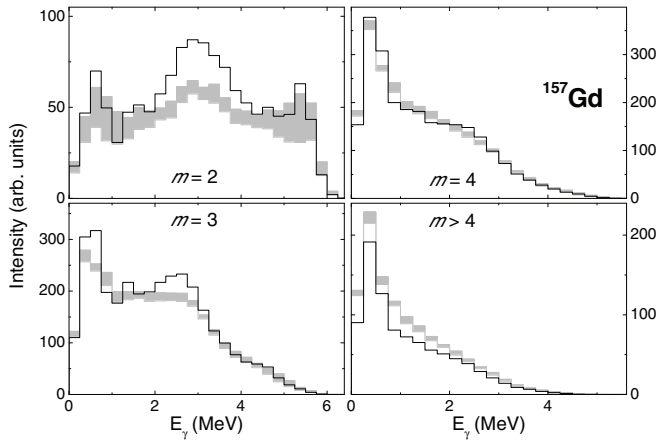

FIG. 11. A comparison between the experimental MSC spectra for ^{157}Gd with simulations. The KMF model was adopted for the $E1$ PSF, while BSFG model for the NLD. For $M1$ PSF a composite $f_{\rm SF}^{(M1)} + f_{\rm SP}^{(M1)} + f_{\rm SM}^{(M1)}$ model, with the SM strength of 2.6 μ_N^2 was used. This model nicely reproduced MSC spectra of ^{153,155}Gd and ^{156,158}Gd. For details see the caption of Fig. 7.

V. COMPARISON WITH OTHER DATA

A. Available data

There are several relevant measurements that provide information on the PSFs at the low-energy tail of GEDR in the $A \sim 150$–165 mass region.

First, there are extensive data from the (n,γ) reaction: (i) values of the PSFs were obtained from the intensities of primary transitions from resonance neutron capture in ^{155,157,159}Gd [32], (ii) information on the PSFs was obtained for two even Gd isotopes, ^{156,158}Gd, from analysis of MSC spectra [4,5], (iii) two-step cascade measurements provided information on the PSFs in ^{163}Dy [11] and ^{160}Tb [51] including the SM parameters, and (iv) information on the total radiation widths of s-wave neutron resonances is available for all stable isotopes [27,52].

Apart from the (n,γ) reaction, data on mixed dipole ($E1$-plus-$M1$) PSFs are available from ^{3}He-induced γ production for $^{160-164}$Dy isotopes [14,15]. In addition, data on γ transitions from the ground states were available from (γ,γ') measurements [44–46] for all even-even rare-earth nuclei and some odd nuclei in the same mass region, including ^{155,157}Gd.

B. Total radiation width

The total radiation width of s-wave neutron resonances, Γ_γ, is the only quantity simulated with the DICEBOX code that depends on the absolute values of the PSFs. All other simulated observables depend only on the ratios of PSFs for different types and multipolarities of transitions; more precisely, on the energy-dependent ratios of PSFs but not on their absolute values. The value of Γ_γ is a sum of contributions of different transition types and multipolarities, in our case $\Gamma_\gamma = \Gamma_\gamma^{(E1)} + \Gamma_\gamma^{(M1)} + \Gamma_\gamma^{(E2)}$. The contribution from the $E2$ strength and the SF $M1$ strength is very small—on the level of a few percent of Γ_γ. The possible contribution of the SP $M1$ is at most about 10% of Γ_γ. The implication is that about 85–95 % of Γ_γ comes from the $E1$ PSF and $M1$ SM strengths. Experimental values of Γ_γ together with predictions of individual models are listed in Table III.

TABLE III. Contribution of different models to the total radiation widths. The SM contribution corresponds to the width of the SM $\Gamma_{\rm SM} = 1.0$ MeV in all cases and the maximum cross section $\sigma_{\rm SM} =$ 0.2, 0.3, 0.7, and 0.7 mb for ^{153,155,157,159}Gd, respectively. The energy of the SM was $E_{\rm SM} = 3.0$ MeV for all isotopes except ^{155}Gd, where it is 2.6 MeV.

$\Gamma_\gamma^{(E1)}$ or $\Gamma_\gamma^{(M1)}$ (meV)	^{153}Gd	^{155}Gd	^{157}Gd	^{159}Gd
SLO	128(4)	127(3)	143(6)	140(9)
KMF	33(1)	35(1)	41(2)	38(3)
MGLO($k = 2$)	34(1)	37(1)	44(2)	40(3)
MGLO($k = 5$)	69(2)	71(2)	83(4)	77(6)
MLO1	60(2)	61(2)	69(3)	63(4)
MLO2	81(2)	81(2)	92(4)	88(6)
MLO3	70(2)	69(2)	77(3)	74(5)
SM	6(1)	12(1)	24(1)	24(2)
Experiment [32]	54(5)	75(6)	88(12)	105(10)
Experiment [52]	55(3)	74(3)	88(12)	90(6)

Based on the absolute values of the predicted $\Gamma_\gamma^{(E1)}$ we can exclude the SLO model for the $E1$ PSF. Noting that the MSC spectra can only be reproduced with the BSFG model for the NLD, $\Gamma_\gamma^{(E1)}$ simulated with the SLO model is at least about 130 meV in all nuclei studied, see Table III. In addition a strong scissors mode, which would contribute from about 20 meV (in ^{193}Gd) to about 60 meV (in ^{157,159}Gd) to the Γ_γ would be required in order to describe the MSC spectra in combination with the SLO model. The simulated values of Γ_γ are by a factor of two or three larger than the experimental ones. The total radiation widths predicted with all other allowed $E1$ models are significantly smaller than with the SLO model, see values in Table III.

As the Table III shows, if we use the same combination of models of $E1$ PSF and NLD with the appropriate parametrization for all of the Gd isotopes studied, then we obtain very similar values of $\Gamma_\gamma^{(E1)}$ independent of the specific isotope. The contribution of the SM with the same parameters $\Gamma_{\rm SM}$ and $\sigma_{\rm SM}$ to Γ_γ is almost isotope independent. As a consequence, if the same model of $E1$ PSF is assumed for all nuclei, the main difference in the simulations arises from the size of the SM which changes with isotope. This difference is at most about 25 meV (if the SLO model for $E1$ is not considered); the total contribution of the SM is at a maximum about 30 meV in ^{157,159}Gd. Experimentally, there is a systematic increase of Γ_γ with mass number A, see Table III. However, in models reproducing the MSC spectra the contribution of the SM alone is responsible for less than half of the increase of Γ_γ. This strongly indicates that there must be a contribution from the $E1$ strength to the observed increase, which further implies that there is no universal parameter-free $E1$ PSF model in the chain of odd Gd isotopes.

It should be emphasized that, except for the MGLO, all of the models considered for the $E1$ strength failed to reproduce the total radiation widths in all nuclei simultaneously. The

success of the MGLO model is due to introduction of the free parameter k, the adjustment of which for individual nuclei can mimic the anticipated change of the $E1$ PSF with A. Any other tested $E1$ PSF model has no free parameter. The value of the parameter k of the MGLO model needed from the requirement to reproduce Γ_γ reasonably well agrees with our results from MSC spectra. Specifically, the increase of the parameter with A, from about $k \approx 2$ for ^{153}Gd to $k \approx 5$ for ^{159}Gd, is needed in both cases.

C. Intensities of $E1$ primary transitions

An acceptable model for the $E1$ PSF should also reproduce the values of the $E1$ PSF obtained from the intensities of primary transitions in the (n, γ) reaction. As seen in Fig. 4, the experimental uncertainties of the $E1$ PSFs are rather large and do not provide any strong restriction on the $E1$ PSF model. Nonetheless, the experimental value for ^{159}Gd [42] seems to provide support for our finding from analysis of MSC spectra and Γ_γ that the $E1$ PSF in this isotope near S_n is higher compared to that for lighter isotopes. The models which are acceptable from our analysis in ^{159}Gd predict a $f^{(E1)}$ that is too small near 5.1 MeV compared to experimental data from Ref. [42], but is still within two standard deviations.

In conclusion, all available experimental data on the $E1$ PSF—total radiation widths, intensities of primary transitions and results from analysis of MSC spectra—seem to be fully compatible with the MGLO model in which the parameter k increases with the the mass of the Gd isotope. On the other hand, all parameter-free $E1$ PSF models seem to be unable to describe all odd Gd isotopes at the same time.

D. Scissors mode

As mentioned in Sec. III B 2, only a fraction of the ground-state transitions is observed in the (γ,γ') reaction on odd nuclei. Comparison of our results with data from (γ,γ') is thus difficult since a correction for the unobserved strength in the (γ,γ') reaction must be performed. Unfortunately, the estimated total $M1$ strength inferred from the measured (γ,γ') data depends significantly on how the correction is performed, see [44,47].

There are additional complications with the comparison of our results with data on the $M1$ strength from other reactions. The strength determined by our analysis consists of both the resonant (SM) and nonresonant (SP + SF) component of $M1$ PSF. We can compare the sum of these components in a restricted interval $E_\gamma = 2.7$–3.7 MeV for which the (γ,γ') data are available for all isotopes. On the other hand, only the resonant part of the $M1$ strength can be compared with the data from Oslo method. For the sake of these comparisons, in Table II we list values of three different sums of reduced transitions probability: $\sum B_{\mathrm{NRF}}(M1)\uparrow$ corresponds to the total (SM + SP + SF) $M1$ strength in the energy interval 2.7–3.7 MeV (the strength in this interval can be compared to the NRF measurements), $\sum B_{\mathrm{NRF}}(\mathrm{SP}+\mathrm{SF})\uparrow$ is a part of $\sum B_{\mathrm{NRF}}(M1)\uparrow$, which corresponds only to the nonresonant SP + SF contribution,

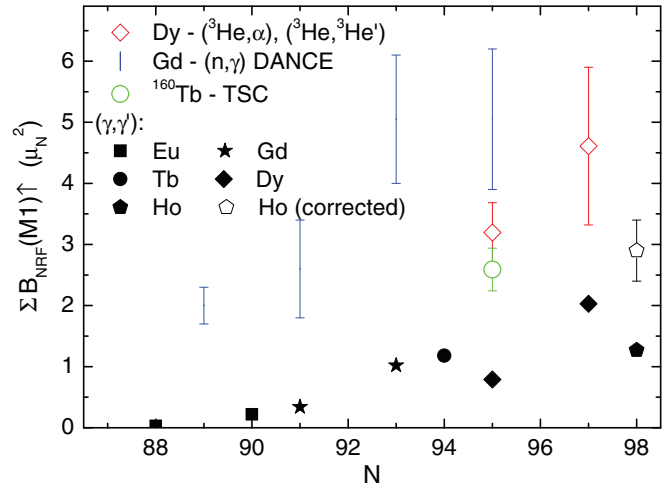

FIG. 12. (Color online) Comparison of reduced $M1$ strength $\Sigma B_{\mathrm{NRF}}(M1)\uparrow$ in odd A isotopes in the Eu-Ho region as a function of the number of neutrons N. Our results are plotted together with NRF data [9,44] and values coming from ^{3}He-induced reactions [14,15]. The strength for odd-odd nucleus ^{160}Tb, obtained in TSC experiment [51], was added.

and $\sum B_{\mathrm{tot}}(\mathrm{SM})\uparrow$ is the total SM strength (summed over all energies). The ranges of reduced transitions probabilities quoted in Table II take into account the requirement to reproduce MSC spectra, as well as the experimental total radiation width (within 1.5 standard deviations), see Table III.

The values of $\sum B_{\mathrm{NRF}}(M1)\uparrow$ obtained from different experiments for odd nuclei in the Gd and Dy region are also plotted in Fig. 12. The reason for the difference between observed (γ,γ') and data from other experiments has already been discussed. Despite a very limited number of experimental points there seems to be a reasonable agreement between (n, γ) data and data from the Oslo method.

This agreement between our data and the Oslo data might be due in part to the restricted interval of E_γ used in Fig. 12—the SM energies and partly also widths are not the same in these two types of experiments. The total SM strengths summed over all γ-ray energies, $\sum B_{\mathrm{tot}}(\mathrm{SM})\uparrow$, for all available nuclei in the Gd-Dy region are shown in Fig. 13. While our and Oslo data seem to reasonably agree for odd nuclei there is a clear disagreement for even-even nuclei with 94 neutrons: ^{158}Gd from the DANCE measurement and ^{160}Dy from the Oslo data. While our results give significantly smaller SM strength in even ^{158}Gd than in neighboring odd Gd isotopes, the Oslo data yield comparable strength in odd and even Dy isotopes. Unfortunately, the SM parameters and therefore the total SM strength determined from the Oslo method depend strongly on the temperature assumed for the $E1$ PSF model in the fit to Oslo experimental data—the total SM strength depends on the product $\Gamma_{\mathrm{SM}} \times \sigma_{\mathrm{SM}}$ which in some cases changes by a factor of more than two in data from the same reaction [14]. The plotted values of $\sum B_{\mathrm{tot}}(\mathrm{SM})\uparrow$ from Oslo data, are from Ref. [15] and correspond to the KMF-T model of $E1$ PSF with $T = 0.3$ MeV.

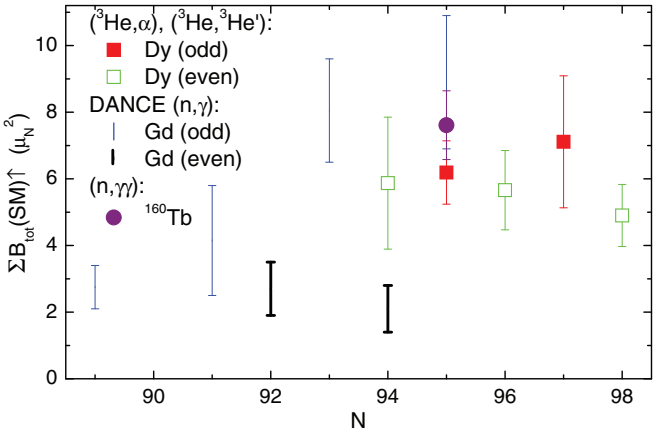

FIG. 13. (Color online) Comparison of the total reduced SM strength $\Sigma B_{\mathrm{tot}}(SM)\uparrow$ for Gd, Tb, and Dy isotopes as a function of the number of neutrons N. Our results (for even-even nuclei see [4,5]) are plotted together with results from ^{3}He-induced reactions [14,15] and from analysis of TSC spectra in odd-odd ^{160}Tb [51].

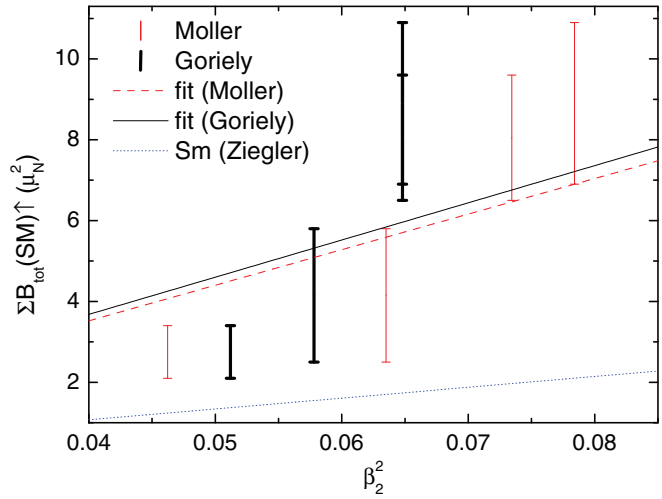

FIG. 14. (Color online) Comparison of the total reduced SM strength $\Sigma B_{\mathrm{tot}}(SM)\uparrow$ as inferred from DANCE measurements of odd Gd isotopes as a function of square of nuclear deformation. Values from two different calculations (Goriely *et al.* [53] and Moller *et al.* [54]) are used for β_2^2. Fits to the experimental data assumed zero strength for nondeformed nuclei. For comparison, the dotted line shows the deformation dependence observed for even Sm isotopes by Ziegler *et al.* [10].

Our data for the $A = 157$–159 region clearly indicate an odd-even effect in the SM strength. A definite conclusion about the same effect for lighter Gd isotopes cannot be made as the broad range allowed for the SM strength in ^{155}Gd partly overlaps with the strength in ^{156}Gd, see Fig. 13. To our knowledge there is no theoretical evidence for such an odd-even effect.

The difference in the strength of the SM in odd Gd isotopes could be, in analogy with ground-state transitions in even-even nuclei, due to the change of nuclear deformation. Unfortunately, the experimental deformation values are not available for odd nuclei. However, values of the deformation parameter β_2^2 are available from two different calculations [53,54], see Table II. The experimental deformations [55] in neighboring even-even nuclei are close to the average value from the two calculations. The results of these two calculations were used to check the deformation dependence of the SM strength, see Fig. 14. From the figure it is evident that the quadratic dependence of the SM strength on deformation is very likely inadequate in odd Gd nuclei and that we are far from the dependence observed in the (γ,γ') experiment on even-even Sm nuclei [10].

VI. SUMMARY

Measurements of γ-ray spectra from strong s-wave neutron resonances on isotopically enriched ^{152,154,156,158}Gd targets were performed using the DANCE detector array at the LANSCE spallation neutron source. The MSC γ-ray spectra obtained from these resonances were used to test the validity of various PSF and NLD models for the odd Gd isotopes.

The main results of our analysis can be summarized as: (i) The energy dependence of the NLD seems to be reasonably well described with the BSFG model, while the dependence predicted by the CT model is highly unlikely. (ii) There is no universal $E1$ model acceptable for a simultaneous description of the MSC spectra and the total radiation width for all four odd Gd isotopes. The MGLO model with different values of the parameter k is the only one of the tested models that can reproduce all experimental data from the (n,γ) reaction. (iii) The experimental total radiation widths of the s-wave neutron resonances indicate that the $E1$ PSF in studied nuclei is almost surely not described by the Lorentzian extrapolation of the GDER. To reach the Lorentzian shape at energies above S_n, the energy dependence must be very steep at E_γ between about 4 and 8 MeV. (iv) The shapes of MSC spectra are compatible with the following two assumptions: first, there is a resonance in $M1$ PSF near 3 MeV, which we identify with the SM, that is built on all levels in nuclei studied, and second, the shape of the SM can be described by the Lorentzian curve. (v) Assuming the Lorentzian shape of the SM, the total strength of the mode in odd Gd isotopes, $\sum B_{\mathrm{tot}}(\mathrm{SM})\uparrow$ increases with the mass number and estimated ground-state deformation. The dependence of the SM strength on nuclear deformation seems to be at variance with the quadratic dependence on β_2^2 observed in even-even nuclei from the (γ,γ') measurement. (vi) Observed SM strength in ^{157,159}Gd significantly exceeds the strength obtained from our previous analysis of the MSC spectra for even-even nuclei ^{156,158}Gd [4,5]. The observed odd-even staggering does not seem to be present in the Oslo data [14,15] and is not anticipated from any theory.

In conclusion, it is evident that there are still many unresolved problems related to the PSFs and the NLD in deformed nuclei. Further study of these quantities is therefore clearly needed. In any case a reasonable simultaneous description of all experimental MSC spectra presented in this work together with the size of expected fluctuations in these spectra indicate that the standard picture of compound nucleus and PSFs is justified for a description of deformed rare-earth nuclei.

ACKNOWLEDGMENTS

This work was supported in part by the U.S. Department of Energy Grants No. DE-NA0001784 and No. DE-FG02-97-ER41042. This work benefited from the use of the LANSCE accelerator and was performed under the auspices of the U.S. Department of Energy at Los Alamos National Laboratory by the Los Alamos National Security, LLC under Contract No. DE-AC52-06NA25396 and LLNL Contract No. DE-AC52-07NA27344. It was also supported by the research plan MSM 0021620859 of the Ministry of Education of the Czech Republic, and Grant No. 13-07117S of the Czech Science Foundation.

[1] M. Heil *et al.*, Nucl. Instrum. Methods Phys. Res. A **459**, 229 (2001).
[2] R. Reifarth *et al.*, Nucl. Instrum. Methods Phys. Res. A **531**, 530 (2004).
[3] P. W. Lisowski and K. F. Schoenberg, Nucl. Instrum. Methods Phys. Res. A **562**, 510 (2006).
[4] A. Chyzh *et al.*, Phys. Rev. C **84**, 014306 (2011).
[5] B. Baramsai *et al.*, Phys. Rev. C **87**, 044609 (2013).
[6] R. R. Hilton, in *Proceedings of International Conference on Selected Topics in Nuclear Structure, Dubna, USSR, 1976*, edited by V. G. Soloviev (JINR, Dubna, 1976).
[7] N. Lo Iudice and F. Palumbo, Phys. Rev. Lett. **41**, 1532 (1978).
[8] D. Bohle *et al.*, Phys. Lett. B **137**, 27 (1984).
[9] U. Kneissl, H. H. Pitz, and A. Zilges, Prog. Part. Nucl. Phys. **37**, 349 (1996).
[10] W. Ziegler, C. Rangacharyulu, A. Richter, and C. Spieler, Phys. Rev. Lett. **65**, 2515 (1990).
[11] M. Krtička *et al.*, Phys. Rev. Lett. **92**, 172501 (2004).
[12] F. Bečvář, P. Cejnar, J. Honzátko, K. Konečný, I. Tomandl and R. E. Chrien, Phys. Rev. C **52**, 1278 (1995).
[13] A. Schiller *et al.*, Phys. Lett. B **633**, 225 (2006).
[14] M. Guttormsen, A. Bagheri, R. Chankova, J. Rekstad, S. Siem, A. Schiller, and A. Voinov, Phys. Rev. C **68**, 064306 (2003).
[15] H. T. Nyhus *et al.*, Phys. Rev. C **81**, 024325 (2010).
[16] M. Jandel *et al.*, Phys. Rev. C **78**, 034609 (2008).
[17] B. Baramsai *et al.*, Phys. Rev. C **85**, 024622 (2012).
[18] P. W. Lisowski *et al.*, Nucl. Sci. Eng. **106**, 208 (1990).
[19] J. M. Wouters *et al.*, IEEE Trans. Nucl. Sci. **53**, 880 (2006).
[20] C. E. Porter and R. G. Thomas, Phys. Rev. **104**, 483 (1956).
[21] F. Bečvář, Nucl. Instrum. Methods Phys. Res. A **417**, 434 (1998).
[22] M. Jandel *et al.*, Nucl. Instrum. Methods Phys. Res. B **261**, 1117 (2007).
[23] R. G. Helmer, Nucl. Data Sheets **107**, 507 (2006).
[24] C. W. Reich, Nucl. Data Sheets **104**, 1 (2005).
[25] R. G. Helmer, Nucl. Data Sheets **103**, 565 (2004).
[26] C. W. Reich, Nucl. Data Sheets **113**, 157 (2012).
[27] R. Capote *et al.*, Nucl. Data Sheets **110**, 3107 (2009).
[28] S. S. Dietrich and B. L. Berman, At. Data and Nucl. Data Tables **38**, 199 (1988).
[29] S. G. Kadmenskij, V. P. Markushev, and V. I. Furman, Sov. J. Nucl. Phys. **37**, 165 (1983).
[30] R. E. Chrien, in *Proceedings of the 5th International School on Neutron Physics, Alushta, USSR, 1987*, edited by B. B. Kolesova and V. R. Sarantseva, JINR Report No. D3, 4, 17-86-747 (JINR, Dubna, 1987).
[31] J. Kopecky, M. Uhl, and R. E. Chrien, Phys. Rev. C **47**, 312 (1993).
[32] J. Kopecky, in *Handbook for Calculations of Nuclear Reaction Data*, Report No. IAEA-TECDOC-1034 (IAEA, Vienna, 1998), p. 97.
[33] T. von Egidy and D. Bucurescu, Phys. Rev. C **72**, 044311 (2005).
[34] T. von Egidy and D. Bucurescu, Phys. Rev. C **80**, 054310 (2009).
[35] A. H. Wapstra and G. Audi, Nucl. Phys. A **432**, 55 (1985).
[36] S. Goriely, Phys. Lett. B **436**, 10 (1998).
[37] S. F. Mughabghab and C. L. Dunford, Phys. Lett. B **487**, 155 (2000).
[38] D. M. Brink, Ph.D. thesis, Oxford University, 1955 (unpublished).
[39] L. M. Bollinger and G. E. Thomas, Phys. Rev. C **2**, 1951 (1970).
[40] A. Voinov, M. Guttormsen, E. Melby, J. Rekstad, A. Schiller, and S. Siem, Phys. Rev. C **63**, 044313 (2001).
[41] F. Iachello, Nucl. Phys. A **358**, 89c (1981).
[42] C. Granja *et al.*, Nucl. Phys. A **724**, 14 (2003).
[43] N. Pietralla *et al.*, Phys. Rev. C **58**, 184 (1998).
[44] A. Nord *et al.*, Phys. Rev. C **67**, 034307 (2003).
[45] A. Nord *et al.*, Phys. Rev. C **54**, 2287 (1996).
[46] J. Margraf *et al.*, Phys. Rev. C **52**, 2429 (1995).
[47] N. Huxel *et al.*, Nucl. Phys. A **645**, 239 (1999).
[48] E. Melby, M. Guttormsen, J. Rekstad, A. Schiller, S. Siem, and A. Voinov, Phys. Rev. C **63**, 044309 (2001).
[49] D. Frekers *et al.*, Phys. Lett. B **244**, 178 (1990).
[50] S. Goriely, Nucl. Phys. A **605**, 28 (1996).
[51] J. Kroll *et al.*, Int. Jour. of Mod. Phys. E **20**, 526 (2011).
[52] S. F. Mughabghab, *Atlas of Neutron Resonances* (Elsevier, Amsterdam, 2006).
[53] S. Goriely, M. Samyn, and J. M. Pearson, Phys. Rev. C **75**, 064312 (2007).
[54] P. Moller, J. R. Nix, W. D. Myers, and W. J. Swiatecki, At. Data and Nucl. Data Tables **59**, 185 (1995).
[55] http://www.nndc.bnl.gov/chart.